SANDIA REPORT

SAND2003-3458
Unlimited Release
Printed September 2003

Reliability Data to Improve High Magnetic Field Coil Design for High Velocity Coilguns

Ronald J. Kaye and Gregory A. Mann

Prepared by
Sandia National Laboratories
Albuquerque, New Mexico 87185 and Livermore, California 94550

Sandia is a multiprogram laboratory operated by Sandia Corporation,
a Lockheed Martin Company, for the United States Department of Energy's
National Nuclear Security Administration under Contract DE-AC04-94AL85000.

Issued by Sandia National Laboratories, operated for the United States Department of Energy by Sandia Corporation.

Available to DOE and DOE contractors from
U.S. Department of Energy
Office of Scientific and Technical Information
P.O. Box 62
Oak Ridge, TN 37831

Telephone: (865)576-8401
Facsimile: (865)576-5728
E-Mail: reports@adonis.osti.gov
Online ordering: http://www.doe.gov/bridge

Available to the public from
U.S. Department of Commerce
National Technical Information Service
5285 Port Royal Rd
Springfield, VA 22161

Telephone: (800)553-6847
Facsimile: (703)605-6900
E-Mail: orders@ntis.fedworld.gov
Online order: http://www.ntis.gov/help/ordermethods.asp?loc=7-4-0#online

SAND2003-3458
Unlimited Release
Printed September 2003

Reliability Data to Improve High Magnetic Field Coil Design for High-Velocity Coilguns

Ronald J. Kaye and Gregory A. Mann
Beam Applications and Initiatives Department
Sandia National Laboratories
P.O. Box 5800
Albuquerque, New Mexico 87185-1182

Abstract

Coilguns have demonstrated their capability to launch projectiles to 1 km/s, and there is interest in their application for long-range precision strike weapons. However, the incorporation of cooling systems for repetitive operation will impact the mechanical design and response of the future coils.

To assess the impact of such changes, an evaluation of the ruggedness and reliability of the existing 50 mm bore coil designed in 1993 was made by repeatedly testing at stress levels associated with operation in a coilgun. A two-coil testbed has been built with a static projectile where each coil is energized by its own capacitor bank. Simulation models of the applied forces generated in this testbed have been created with the SLINGSHOT circuit code to obtain loads equivalent to the worst-case anticipated in a 50 mm coilgun that could launch a 236 g projectile to 2 km/s.

Bench measurements of the seven remaining coils built in 1993 have been used to evaluate which coils were viable for testing, and only one was found defective. Measurements of the gradient of the effective coil inductance in the presence of the projectile were compared to values from SLINGSHOT, and the agreement is excellent.

Repeated testing of the HFC5 coil built in 1993 has demonstrated no failures after 205 shots, which is an order of magnitude greater than any number achieved in previous testing. Although this testing has only been done on two coils, the results are encouraging as it demonstrates there are no fundamental weak links in the design that will cause a very early failure. Several recommendations for future coil designs are suggested based on observations of this study.

Intentionally Left Blank

Contents

Figures

Tables

Nomenclature

GN	gigaNewton
kbar	1000 bars or atmospheres pressure
kgee	1000 time acceleration of gravity
lbf	pounds force
MN	megaNewton
SNL	Sandia National Laboratories

Introduction

Coilguns are electromagnetic guns that use the Lorentz (JxB) force to accelerate a projectile with a conducting armature to high speed. Coilguns have potential application in the next-generation long-range artillery guns for land-based and naval platforms. A study conducted for the U.S. Navy has prompted great interest in this technology for gun and launch applications, particularly for long-range precision strike. [1] In this study it was shown that such guns could launch large (60 kg) warheads or reconnaissance devices at velocities > 2 km/s to targets at 100's of nautical miles range at 50 nautical miles/minute. Electromagnetic launch has several advantages compared to conventional technology that uses propellant:

- Reduce detection due to low-signature launch (no smoke, flash, infrared or sound from expanding gasses).
- Eliminate propellants which improves safety on launch platforms.
- Simplify ammunition logistics tail & reduce operation and maintenance costs by the elimination of propellant.
- Increase projectile range.
- Increase flexibility of target zoning through continuously adjustable stored electric energy.
- Improve targeting accuracy through feedback-control of muzzle launch speed.
- Adjustable, tailored acceleration capability for soft-launch of surveillance/recon sensors.

Coilguns that have been developed at Sandia National Laboratories consist of short-length, solenoidal electromagnets that are stacked end-to-end to form a barrel as shown in Figure 1. The coils are energized sequentially to create a wave of magnetic energy moving from breech to muzzle. This transient wave generates an induced current in a movable armature coil attached to the launched projectile. The induced current and barrel coil's magnetic field generate Lorentz forces that accelerate and compress the armature. Likewise, the windings of the barrel coil sustain a large radial and reaction axial force.

Each of the coils shown in Figure 1 is energized by its own capacitor bank. This is shown schematically in Figure 2 for three coils. To create the traveling magnetic wave in the barrel that is synchronous with the location of the armature, a real-time detector locates the projectile and the gun firing system generates the trigger to the main closing switches of the individual banks. The launch acceleration can be tailored to the needs of the projectile since the stored energy in each bank is adjustable. A uniform acceleration profile that is near the projectile's maximum yields the desired muzzle velocity with the shortest length gun.

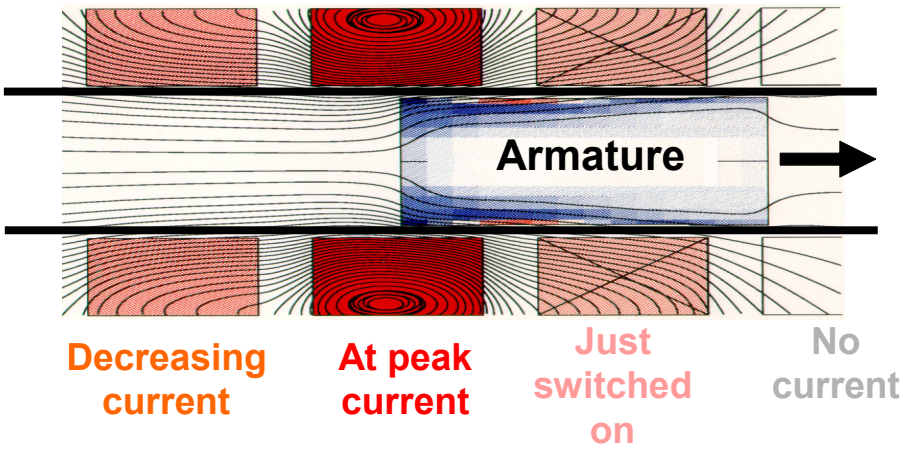

Figure 1. Cross-section view of axisymmetric coilgun with contours of magnetic vector potential that is similar to flux lines. The intensity of the red color represents the magnitude of the current in each coil.

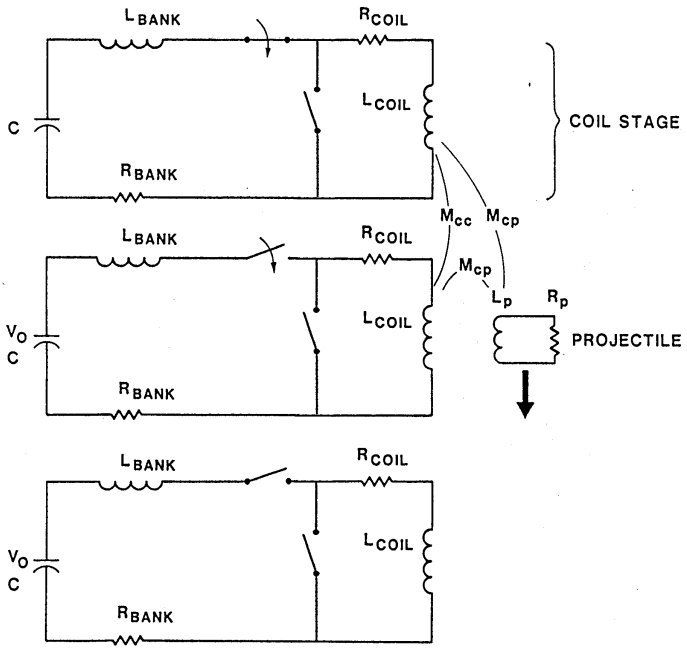

Figure 2. Each coil of the gun is energized by its own capacitor bank. The electrical schematic represents the circuit for a coilgun with three barrel coils where the current is flowing to the top coil, the switch of the second stage bank is about to close, and no current is flowing yet in the third stage coil.

One application considered for the coilgun is long-range fire support from a destroyer-class ship. The scenario developed for a recent feasibility study showed that the gun magazine might hold as many as 1400 rounds as shown in Figure 3. Assuming the ship receives as many as 7 loadouts of ammunition prior to gun servicing, the barrel must be capable of reliably firing 10,000 shots. Comparing to current-technology propellant guns, the service life of a 5-inch/54 Mk19 (Mod 0 or 1) barrel of a Mk 45 5-inch/54 naval

gun that fires rounds at about 800 m/s is 6,000 to 10,000 equivalent standard rounds. For a coilgun comprised of a few hundred coils, the individual coil lifetime will need to be several times this value. The actual number will depend upon the shot life statistics of the tested coil design and failure mechanisms.

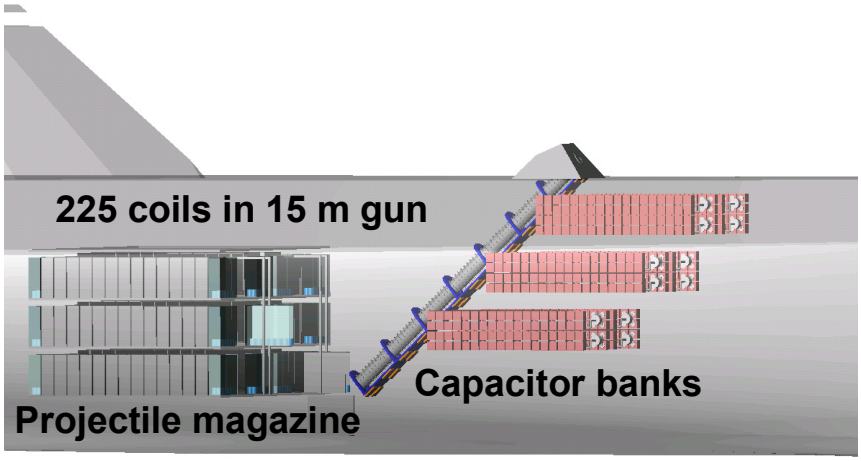

Figure 3. Section view of fixed-position coilgun in hull of destroyer with capacitor bank energy store and 1400-round projectile magazine. Although gun has fixed orientation, the projectiles can maneuver for cross and down range capability.

Our previous work in the early 1990's had successfully designed and tested nested helix coils in a 1.6 m long coilgun accelerating 50 mm diameter, 237g armatures up to 1 km/s.[2] The details of this coils' construction and the coilgun are shown in Figure 4. The high-field coil was tested only in the last 5 gun stages of the 35 stage coilgun. The first 30 coils were an earlier design capable of lower field levels and energy.

The nested helix uses multiple layers of wire to reduce the current density and ohmic heating with each layer supported by a discrete reinforcement shell to support the radial and axial loads. To limit the temperature rise in the winding from each current pulse, the helical winding was constructed of litz cable to provide as much conductor in each layer as possible. Litz cable is constructed of insulated wire strands twisted in such a way that results in a uniform current distribution across them. In this design Kevlar-49 fiber was integrated into the litz cable winding to maintain the cable geometry and preserve the integrity of the electrical insulation [3].

Each of the winding layers was supported by a Nextel 440 fiber/epoxy composite reinforcing shell that captured the round cable within machined threads to distribute the axial recoil loads.[4] These tests demonstrated the ability of the shells to restrain the large radial and axial loads and keep structure strains to a few percent. However, only about 12 gun shots were conducted due to the length of the program.

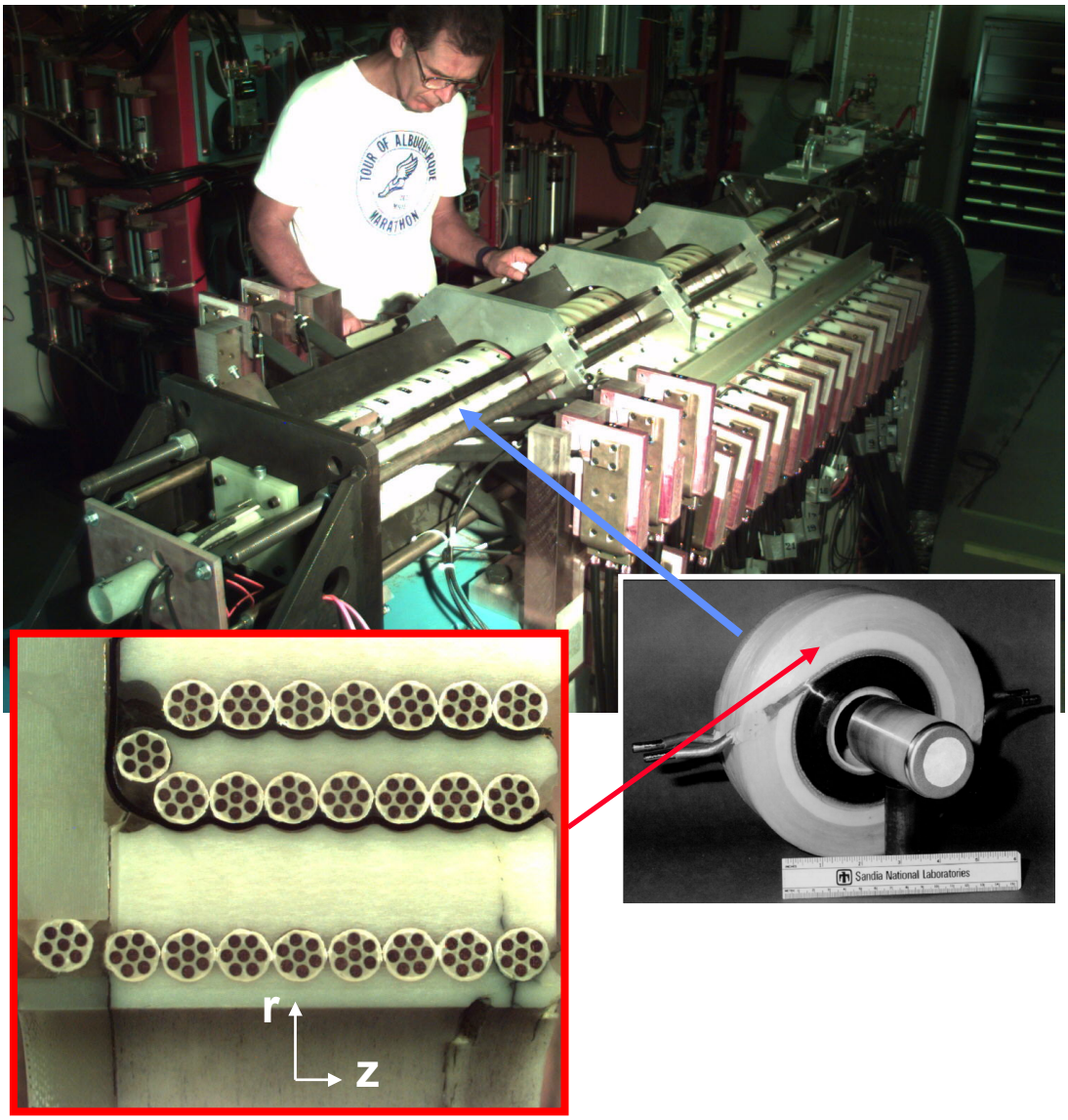

Figure 4. Nested helix coil tested in the last 5 stages of the 40 stage coilgun that accelerated 237 g, 50 mm diameter projectiles to 1 km/s. The nested helix coils achieved an average pressure over the base of the armature of 1 kbar.

Results of these tests are shown in Figure 5 where data from the laser ranger that tracked the projectile during launch is plotted with results of calculations from our SLINGSHOT circuit code that simulates coilgun performance. Two tests are shown with different projectile masses and orientation of the magnetic field in the last five coils of the gun. Parallel field indicates the axial magnetic field direction of these last 5 coils is in the same direction as the field in the first 30 stages, while reversed means that the field in the latter stages is 180° opposite from that in the first stages. Operation with reversed field permitted testing the coil at greater stress levels than anticipated in normal duty operation with parallel fields.

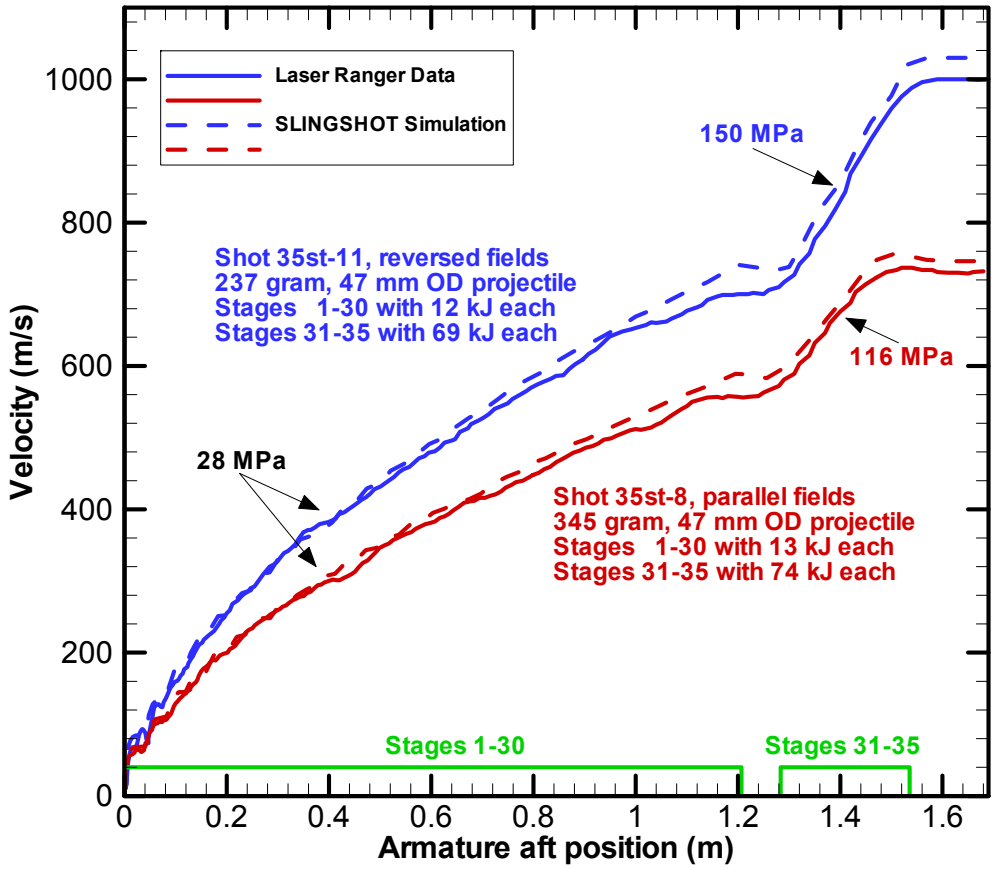

Figure 5. Calculation and data from two 1993 tests with aluminum armatures in the 50 mm coilgun. For the blue curves marked reversed fields, the magnetic field in stages 31 thru 35 is opposite the direction of field in stages 1-30.

The agreement between the velocity data and the calculations is excellent. This gives us confidence in the ability to use the code for design of components at this and greater scale size. The SLINGSHOT code was also used as a design tool during the development of the high field coil. Forces developed within the coil during launch were output to a finite-element stress analysis code to evaluate the elastic response. Conditions during the operation of the last five stages were used as a baseline stress level for the coil testing described below.

The purpose of this study is to further the development of coils for coilguns to achieve the requirements of future applications. These applications will require operation with the same 30 Tesla magnetic field strength, but with bore diameters ranging from 100 to 300 mm and firing rates of several shots per minute. Because of the energy dissipated in the coils, heat must be rejected through a coolant or transport mechanism for repetitive operation. The incorporation of a cooling system will impact the mechanical design and response of the future coils. To assess the impact of such changes, an understanding of the ruggedness and reliability of the existing 50 mm bore coil is necessary.

Data is available from the 1993 coilgun development from both individual coil testing and coilgun operation. Each of the high-field coils, designated model HFC5, were evaluated in qualification testing in a testbed with a static projectile at 100% of gun operation stress level following fabrication. Additionally, one coil was tested with 21 shots at stress levels greater than 33% of gun operation stress. These tests included several shots at 100% and 150% gun operation stress levels. Once the gun was assembled, 12 coilgun shots were conducted with these coils at or near 100% stress levels. Program funding did not permit additional testing.

Near the end of gun testing, one coil of the 10 coils fabricated failed internally. Post test inspection indicated that the region of the second reinforcing shell where the litz cable transitions from the inner to middle winding layer lacked sufficient strength due to the space allocated for the transition between layers. Other areas of the coil had maintained their structural and electrical integrity. Subsequent analysis and recommendations for improvement of the transition weakness is described below.

While the testing in 1993 demonstrated the performance of the coil and one possible failure mechanism, there was insufficient data to make any conclusion on possible lifetime of the coils. Of particular interest for this study is the identification of other possible failure mechanisms that may only occur due to repeated testing. These include breakage of the winding conductor due to work hardening from mechanical fatigue or electrical insulation breakdown due to abrasion. Both of these may arise from the pressure of the applied stress to the winding and micro-movement of the coil's strain response.

To quantify the lifetime and possible associated failure mechanisms of the existing coil design, a two-coil testbed has been constructed with a fixed, static projectile. This testbed will repeatedly stress the coil-under-test to the mechanical, electrical, and thermal loads anticipated in operation of a coilgun of equivalent size. The two coils are energized simultaneously to maximize the loading on the muzzle-end coil which contains the projectile held static in a position for maximum thrust. The geometry simulates the forces and the mechanical boundary conditions that occur in the coils of a multi-stage coilgun. The life data and failure mechanisms generated from this study can then be compared to results of other high-field coils used for high-magnetic field physics experiments to determine if there is commonality in lifetime for equivalent field or mechanisms of failure.

1. Description of Coil and Required Loads

As described in the section above and shown in Figure 4, the coil consists of a litz cable winding reinforced by fiber composite shells. The winding has two cables wound in parallel but offset from each other 180° about the coil axis. Each of these cables has its own set of feeds which are connected in parallel to the current source. This can be seen in the section views of the CAD model shown in Figure 7.

The litz cable is a 6-on-1 spiral winding of 1 mm diameter (18 AWG) copper (UNS C11000) wires, each with a triple coat of Phelps Dodge Armored Poly-Thermaleze 2000, and a 0.13 mm thick braid of Dupont Kevlar 49. Tows of Kevlar are wound with the braid-covered wire at a 90 mm pitch and held together by an additional Kevlar braid forming the 5 mm OD cable.

Table 1. Mechanical and Electrical Parameters of HFC5 Coil

Winding ID, OD, length	57 mm, 114 mm, 40 mm
Structure ID, OD, length	51 mm, 188 mm, 53 mm
Number of turns	11.5
Winding inductance (2.5 kHz)	9.1 uH
Winding resistance (2.5 kHz)	5.9 mOhms

Qualification of HFC5 Coil Prior to Testing

All the seven HFC5 coils remaining from the coilgun development effort in 1993 had been previously tested, and two had damage to their feeds during the 10 years of storage. To determine the viability of the coils prior to testing with capacitor banks, the inductance and resistance of each coil was measured at several frequencies to evaluate the condition of the litz cable and the cable-to-feed connection. This was done using an HP 4192A Low-Frequency Impedance Analyzer with the coil electrically isolated from structures and other coils. Additionally, coil inductance and resistance measurements were made with a 50 mm diameter, 86 mm long, 7075-T6 aluminum projectile positioned over a range of axial distances from the coil. This data provided equivalent circuit and coupling parameters to compare to those generated by the SLINGSHOT code.

Coil inductance and resistance data for four separate coils at 2.5 kHz frequency are shown in Figure 8. Abscissa values are the distance between the axial center of the projectile and the axial midplane of the coil with best coupling at overlapping centers. At this projectile location, the inductance seen at the terminals of the coil is reduced by the mutual coupling to the projectile, and the apparent coil resistance is increased. As the projectile is moved out of the coil, the inductance and resistance approach the coil's self

inductance and resistance. The values predicted by the SLINGSHOT code are also shown and are in good agreement with the code with coil self inductance within 2.5% and coil uncoupled resistance at 15%. Note that ordinate axes are not zero based.

One coil showed an anomalously high resistance with was believed to be due to damaged connections to the feeds. All measurements were repeatable and uncertainties for inductance and resistance measurements are estimated to be within 3%.

Another cross check of the SLINGSHOT code was made using the inductance measurements of the coil coupled to the projectile. With a solid projectile, the currents induces in it are eddy currents and the distribution of these is modeled by numerous, parallel, single-turns loops.[5] The total thrust force can be determined by summing the force from each of the *N* projectile loops from the equation:

$$F_z = \sum_{j=1}^{N} I_c I_{pj} \frac{dM_{cpj}}{dz} = \tfrac{1}{2} I_c^2 \sum_{j=1}^{N} 2 \frac{I_{pj}}{I_c} \frac{dM_{cpj}}{dz} \qquad \text{(Eq. 1)}$$

where I_c is the coil current, I_{pj} is the current in the j^{th} projectile loop, and M_{cpj} is the mutual inductance between the coil and that loop.

The effective inductance seen at the terminals of the coil can be expressed as:

$$L_{eff} = \frac{1}{\left([L]^{-1} \right)_{1,1}} \qquad \text{(Eq. 2)}$$

where the subscript *1,1* refers to the first row, first column of the inverse of the inductance coefficient matrix, *L*, for the system of circuit equations where the self and mutual inductance coefficients of the barrel coil equation are in the first row. This is valid for a condition where either the current is zero, such as switching time, or for a good-conductor material projectile material such as aluminum.

It can be shown, albeit with significant algebra,

$$\frac{dL_{eff}}{dz} = \frac{d/dz \left| [L] \right|}{Adj\left(L_{1,1} \right)} = \sum_{j=1}^{N} 2 \frac{I_{pj}}{I_c} \frac{dM_{cpj}}{dz} \qquad \text{(Eq. 3)}$$

where *Adj* is the adjoint and | | represents the determinant. This results in the equation:

$$F_z = \tfrac{1}{2} \frac{dL_{eff}}{dz} I_c^2 \qquad \text{(Eq. 4)}$$

Using the projectile thrust generated at peak current, an effective inductance for the coil and projectile was calculated with Eq. 4 for a range of projectile positions relative to the center of the coil. This calculated inductance gradient is compared to the measured gradient for four of the HFC5 coils in Figure 6. There is very good agreement between the SLINGSHOT code calculated values and the data. The method of calculating the forces between coils and projectile elements to generate this inductance gradient is the same as used for the forces on all coil elements in the code. Therefore, the agreement validates the use of the code for the force predictions for this coil lifetime study.

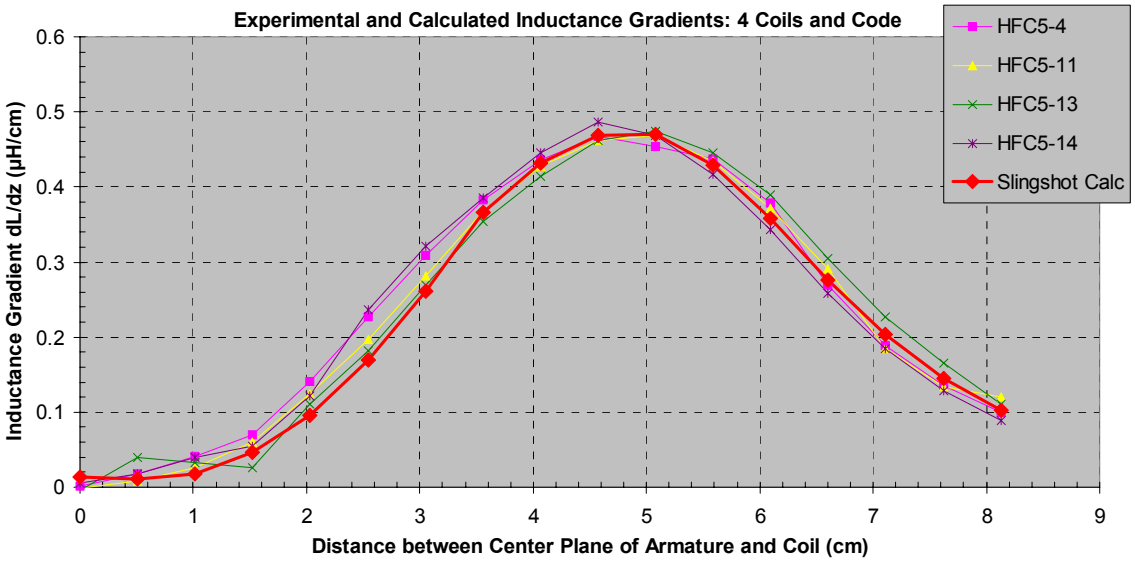

Figure 6. Calculated and four measured gradients of the effective inductance at the coil terminals as a function of the axial distance between the center of the 86 mm aluminum projectile and the midplane of the coil.

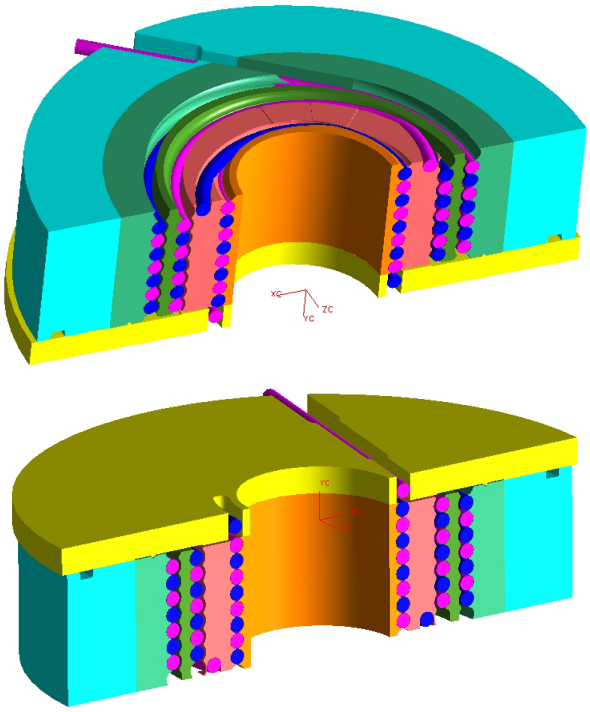

Figure 7. Half-sections of models of the breech (top) and muzzle ends of the model HFC5 coil. The two separate litz cables are colored dark blue and magenta.

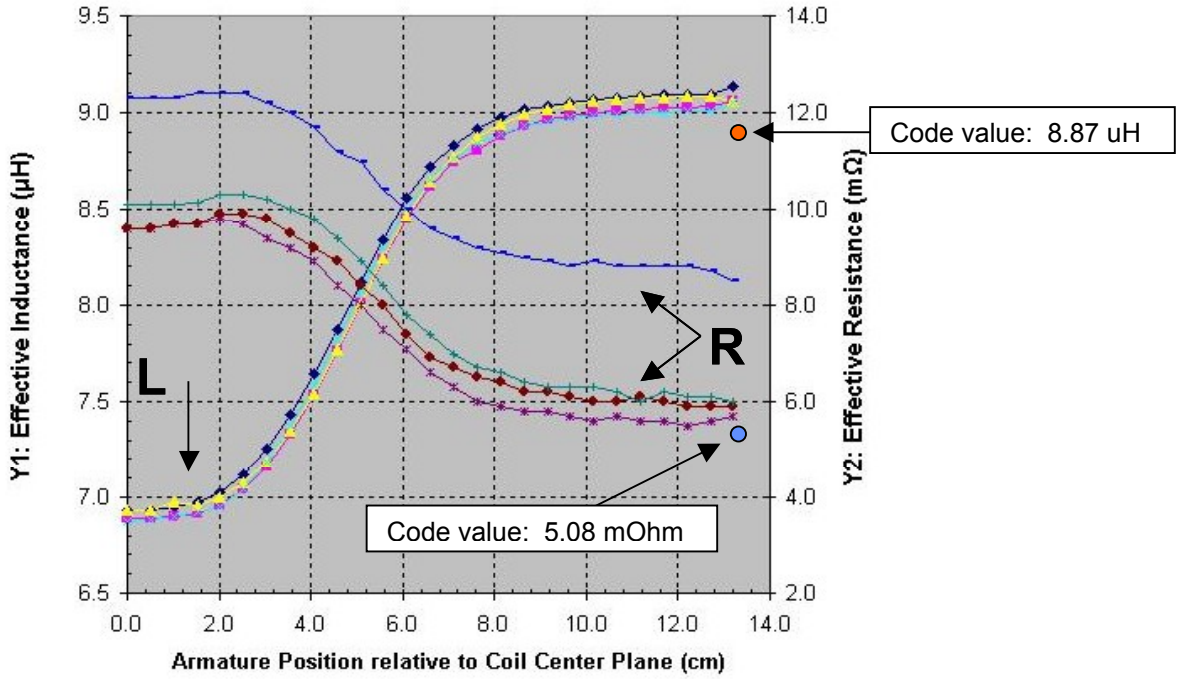

Figure 8. Inductance and resistance at terminals of four separate coils with center of projectile positioned relative to coil midplane. Coil with anomalously high resistance was eliminated from pulse testing. Coil inductance and resistance predicted by SLINGSHOT code shown when uncoupled to projectile.

Loads on Coil During Coilgun Operation

One application planned for the existing 50 mm coil is an 80-stage coilgun that would launch a few hundred gram projectile to between 2 and 2.5 km/s to demonstrate predicted performance and firing control at high-velocity. Calculations with our coilgun circuit simulation code, SLINGSHOT, have determined the mechanical and thermal loads anticipated in that coilgun launching a 238 g, 50 mm projectile to 2.1 km/s. The velocity and acceleration profile are shown in Figure 9. The large change in acceleration at 2.3 m is due to a reversal of the magnetic field direction in coil stages 41-80 to opposite that in stages 1-40.

While the field reversal effectively boosts the acceleration for this gun configuration, it also exacerbated the axial forces on the coils in this region due to the large repulsion between stages 40 and 41. As seen in Figure 10, most of the coils in the gun experience a peak axial force of -0.6 MN or less (negative is toward the gun breech), but values for coils at the reversal range from –1.3 to +1.05 MN. Total radial force on these coils is only marginally affected compared to the balance of the gun with peak values near 2.6 MN.

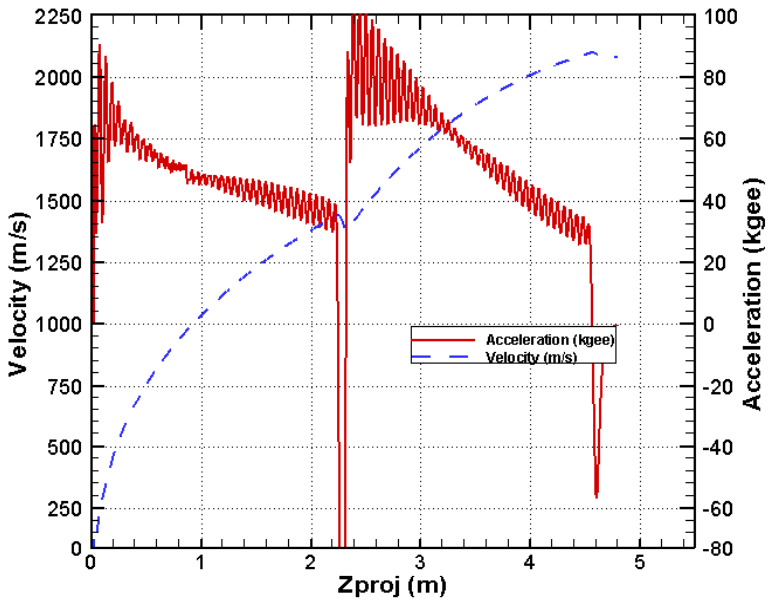

Figure 9. Calculated velocity of 238 g projectile accelerated in a 50 mm coilgun for demonstration of high-speed capability.

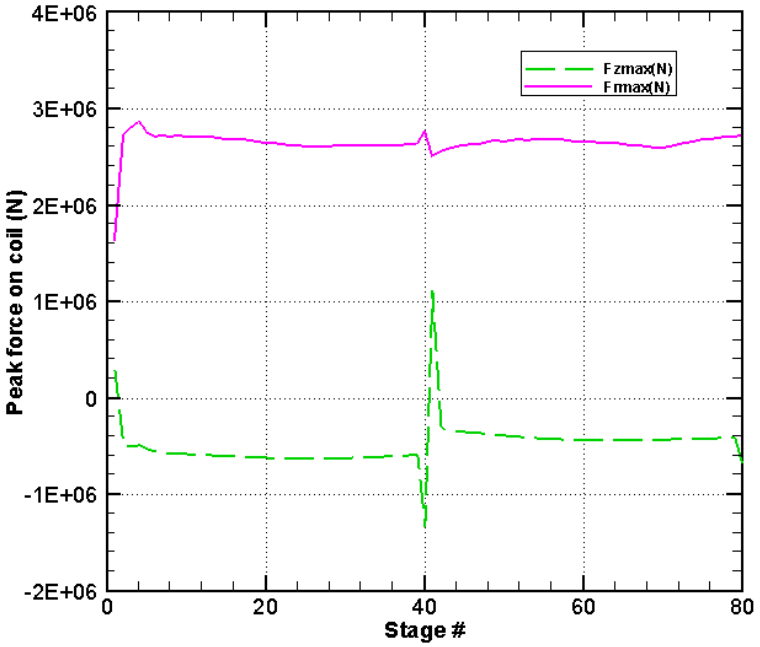

Figure 10. Peak values of radial and axial forces in each of the 80 coil stages of 50 mm coilgun with field reversal at stage 41.

Aside from the peak axial values near the field reversal, these force values are very similar to those calculated for normal operation of the HFC5 coils tested in the 35-stage gun in 1993 with peak radial force at 2.6 MN and peak axial force of –0.64 MN. Given these loads as requirements, a priority for the static testbed was made to limit the radial force level to 2.6 MN (the coil's design load), and accept the axial force level achievable with a two-coil test with parallel fields. While these axial load values are less than those generated with reversed fields, the body forces on the nearest turns of the two coils' windings are attracting each other placing them mechanically in tension with the rest of their winding. This is the more severe test for the turns at the ends of the winding. Additional testing will follow as time permits with reversed fields which generate the higher axial loads.

2. Coil Testbed With Static Projectile

To quantify the lifetime of the HFC5 coil design at the required loads, a two-coil testbed has been constructed with a fixed, static projectile. The physical arrangement of the coils is shown in Figure 11 with a bore tube partially cut away to show the projectile. Figure 12 shows the cross-section of the coils and projectile in the model space of SLINGSHOT. The contours are values of radius times the azimuthal component of the magnetic vector potential (rA_θ), which is similar to the representation of flux lines of the magnetic field. The projectile is a partially hollowed rod of aluminum and modeled as numerous, parallel conducting loops so that the current distribution in the projectile can be determined.

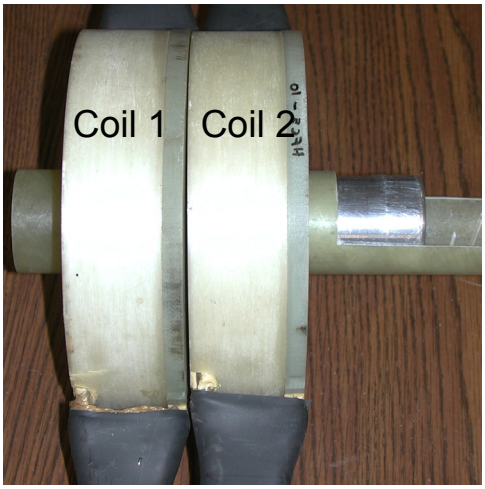

Figure 11. Physical geometry of the two HFC5 coils with the aft end of the 50 mm projectile located at the midplane of coil 2.

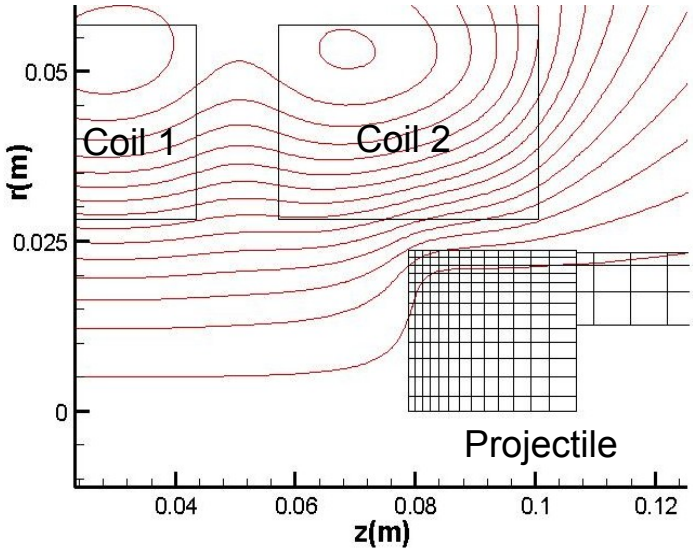

Figure 12. Model space in SLINGSHOT code of two-stage coil testbed with projectile. Contour are values of vector potential, similar to flux lines.

Figure 13 shows how the coils are held in a rigid structure to maintain their alignment and contain their axial forces as well as those applied to the projectile. The coils are surrounded by dielectric blocks and held in alignment by radial steel bars. The entire assembly is held in compression and fastened to a base plate.

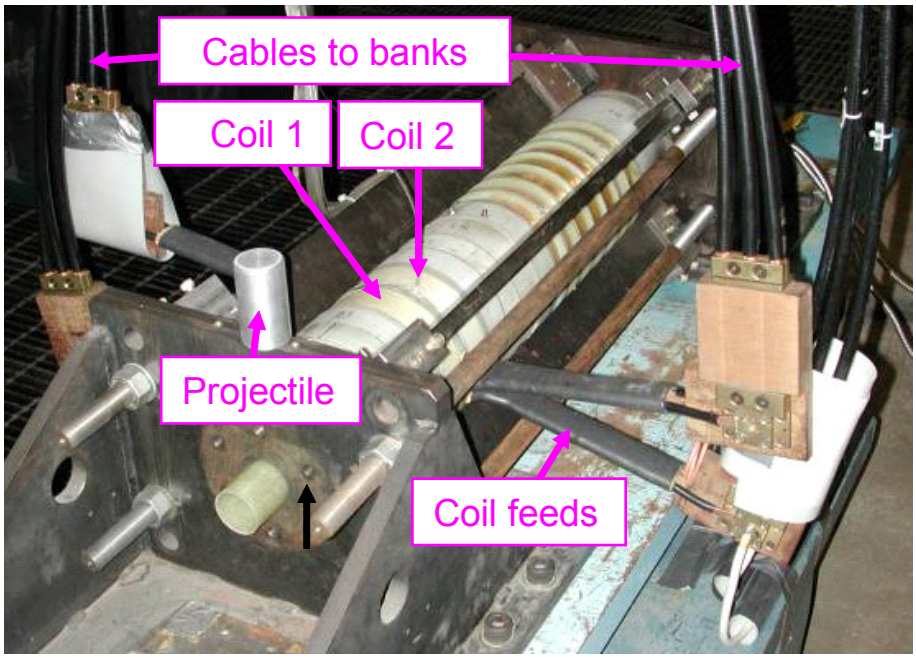

Figure 13. Coils in support structure with feeds connected to coaxial cables to capacitor banks.

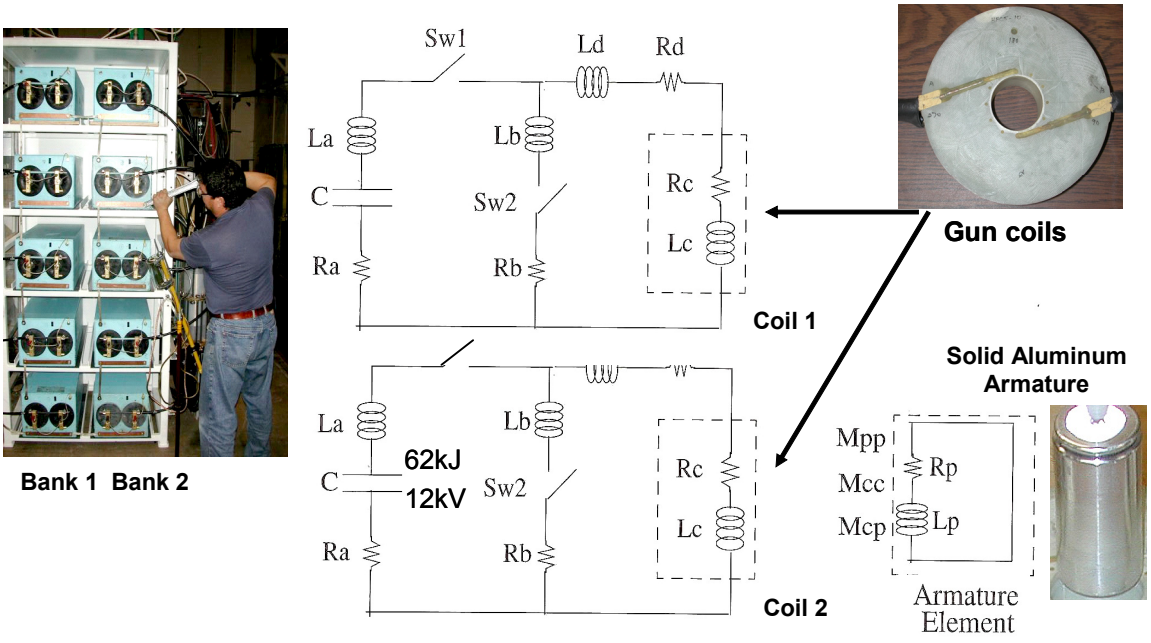

Figure 14. Circuit diagram and components of testbed power circuit.

The electrical circuit for powering the coils is shown in Figure 14 where each of the coils is energized by its own 5-capacitor bank through ignitron switches. Parameters for the circuits are given in Table 2. The switch SW2 is used as a crowbar switch to prevent ringing of the current in the capacitor leg of the circuit and prevent a large voltage reversal on the capacitors which reduces their lifetime. However, the crowbar resistor, Rb, normally a very small value, has been sized to be sufficiently large to extract the energy from the coil quickly after peak current is established to minimize coil heating. In operation of a coilgun, it is desirable to have the coil current decrease as rapidly as the rise since long duration current has no value once the projectile has decoupled magnetically from that coil. Therefore this resistor, formed from multiple layers of stainless steel sheet, has been sized to absorb the bulk of the energy stored in each shot.

Table 2. Parameters of Circuit That Drive Testbed Coils

C	5 each, 172 uF, 21.7 kV capacitors
La, Ra	88 nH, 66 mOhm
Lb, Rb	190 nH, 56 mOhm
Lc, Rc	9.1 uH, 5.9 mOhms at 2.5 kHz
Ld, Rd	61 nH, 44 mOhms in Bank 1 75 nH, 54 mOhms in Bank 2
SW1, SW2	National NL 2888A ignitron
Magnetic coupling	0.36 with aft end projectile at midplane of coil 2
Projectile	50.8 mm OD, 86.5 mm long, 7075-T6 aluminum

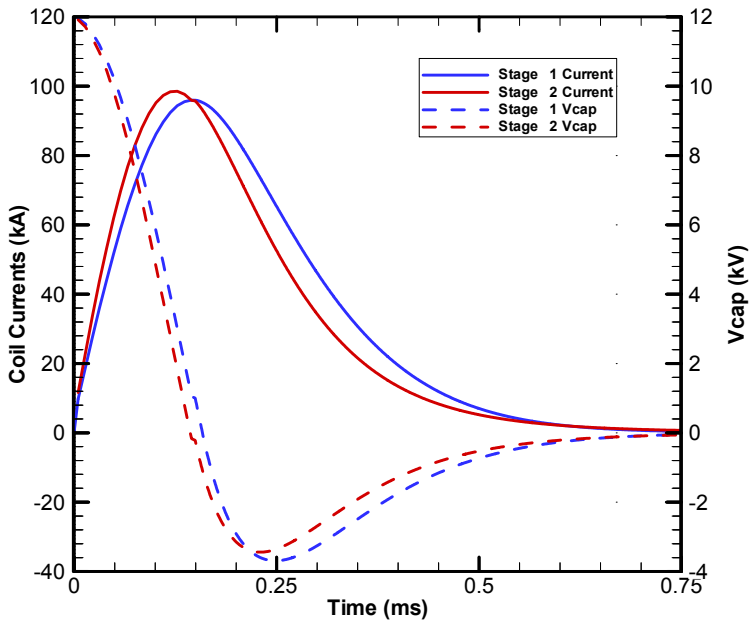

Figure 15. Calculated coil currents and bank capacitor voltages for each bank .

Coil current and capacitor voltage waveforms from SLINGSHOT calculations for the two coil stages are shown in Figure 15. The main switches, SW1, for each bank are closed simultaneously at zero time. As the projectile is more closely magnetically coupled to the Coil 2, the effective inductance seen by Bank 2 is lower resulting in the shorter current risetime to peak. Crowbar switch, SW2, is closed when the capacitor voltage reaches zero for each bank.

The 100 kA current levels shown in Figure 15 generate forces on Coil 2, the coil-under-test, at levels that are 100% of the radial force test requirement of 2.6 MN. The distribution of force is calculated from JxB Lorentz force density and is shown in Figure 16. The spatial distribution of the magnetic field is determined from a two-dimensional solution of magnetic vector potential using the currents in the SLINGSHOT zones at the time of peak current in Coil 2. The temperature noted on each coil is the final temperature after decay of the entire current pulse.

The coils are modeled as single zones with assumption of uniform current density over their cross-section in SLINGSHOT. This is reasonable since the litz cables are distributed through out the cross-section. The radial force density profile in the coils is therefore proportional to the distribution of the axial component of the magnetic field, and the axial force density profile is likewise proportional to the radial field component. The projectile is modeled with more finely spaced single-turns zones, all electrically in parallel, each with assumed uniform current density. The force distribution seen in the aft section of the projectile is a result of the distribution of currents in those zones as calculated by SLINGSHOT circuit simulation, and the resulting magnetic field distribution from all currents.

Total radial and axial force on each coil is shown on each coil with a representative vector. The test configuration meets the requirement of 2.6 MN radial force and the axial force exceeds the -0.64 MN axial load typical of most of the coilgun where the field is parallel as discussed in Figure 9 and Figure 10. Although the axial load is less than the -1.3 MN load at the location of the field reversal in that coilgun, that load condition will be met if the testbed is configured with reversed fields.

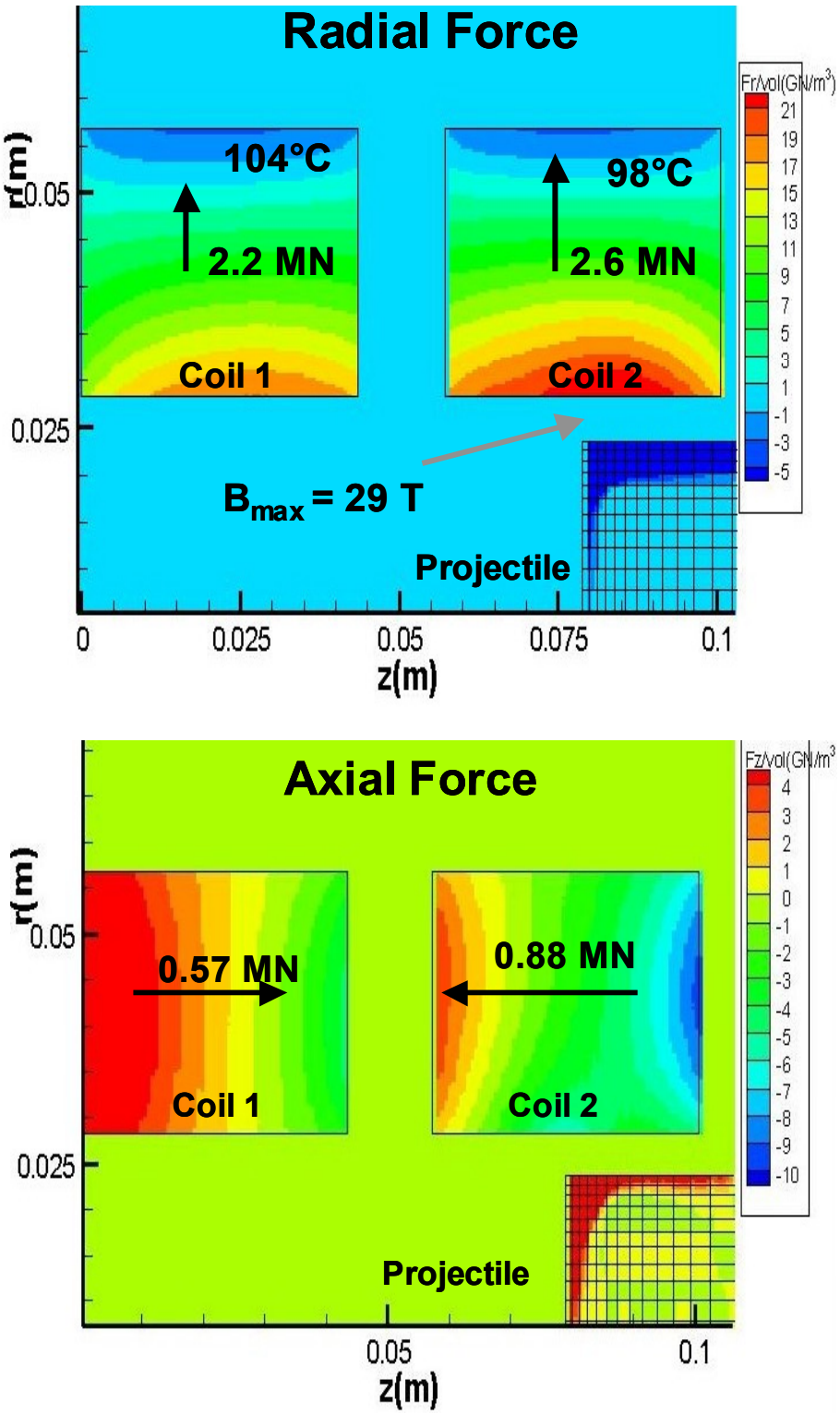

Figure 16. Radial and axial force/volume distributions (GN/m^3) and total integrated loads in coils and projectile of two-stage static testbed at time of peak current in Coil 2 for 62 kJ stored in each stage bank.

3. Results of Coil Testing

Test plan

Because of the known potential failure at the layer-to-layer transition of the litz cable at a coil stress level associated with 62 kJ stored per stage (100% gun stress level), this work focused on obtaining a large number of shots just below that level to determine if other failure mechanisms could be identified. Because of the short length of time for this late-start LDRD, it was proposed to test a coil between the 50% and 100% gun stress levels stepping in 10% increments. At each step 50 shots are taken with time allowed between shots such that the temperature of the bulk composite between Coils 1 and 2 is maintained below 28°C. Waveforms for voltage at the coil terminals and current to both coils are closely monitored to look for coil degradation and the possible onset of coil failure.

Between these tests, additional low-energy tests are conducted with Coil 2 only at the 10% gun stress level (6.2 kJ stored) where the crowbar switch, SW2, is NOT closed at time of peak current to allow the current to ring for several cycles. From the ringing current data waveform the total series equivalent resistance and inductance of the circuit can be unfolded to monitor for change in the condition of the coil. For these low-energy ringing tests, the projectile is removed from the setup and Coil 1 remains an open circuit.

The first two coils selected for Coil 1 and 2 of the testbed were coils HFC5-12 and HFC5-13. These were selected because they were believed to possibly be weakened since their feeds were bent about 10° out of alignment during long-term storage. It was assumed that these might fail after a low number of shots if the feed-to-litz cable joint had been damaged such that it would not support high current, although it did not show evidence of high loss in the bench measurements.

Shot History to Date

Coil HFC5-13 is currently being tested as Coil 2 in the static testbed and has received 205 cumulative shot with the distribution of shots shown in Figure 17. There has been no evidence of coil degradation to date, and the coil will be tested to a minimum of 300 shots or failure.

Before, during, and after testing at a given gun stress level, additional tests are conducted at 10% gun stress level where the current in Coil 2 is allowed to ring at the natural frequency of the circuit, about 1.8 kHz. Waveforms from Rogowski probe 2W is shown in Figure 18 after selected numbers of tests. Aside from the slight change in waveform the from the initial condition test, there has been virtually no change to the coil inductance and resistance. The Rogowski probe signal, proportional to dI/dt, is used as a diagnostic because it is more sensitive to pickup of an arcing condition such as might occur if a wire within the litz cable were breaking or if the wires of the litz cable were shorting to one another. There is no evidence of this in the waveform data. Should such a condition occur, it would persist at all energy levels of operation.

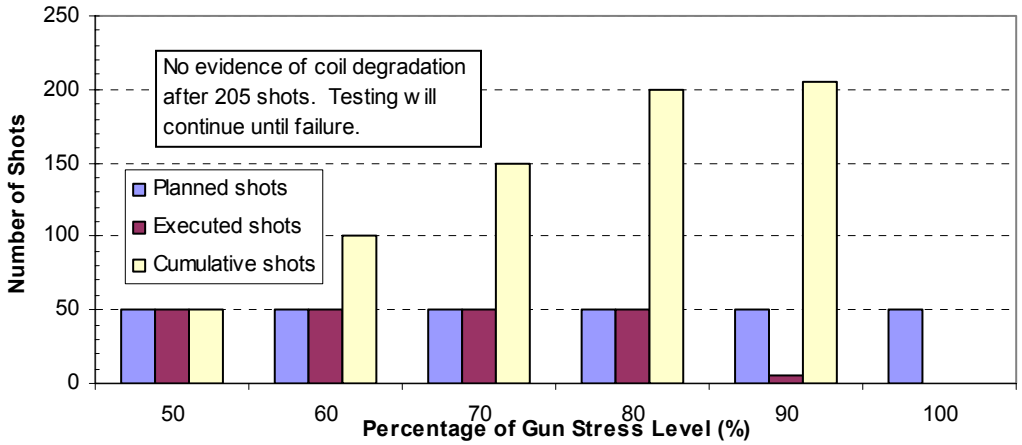

Figure 17. Distribution of shots on Coil HFC5-13 in Coil 2 position of testbed. . 100% gun stress level corresponds to 62 kJ of energy stored in capacitor bank of each coil. Coil is fully functional after 205 shots and testing will continue.

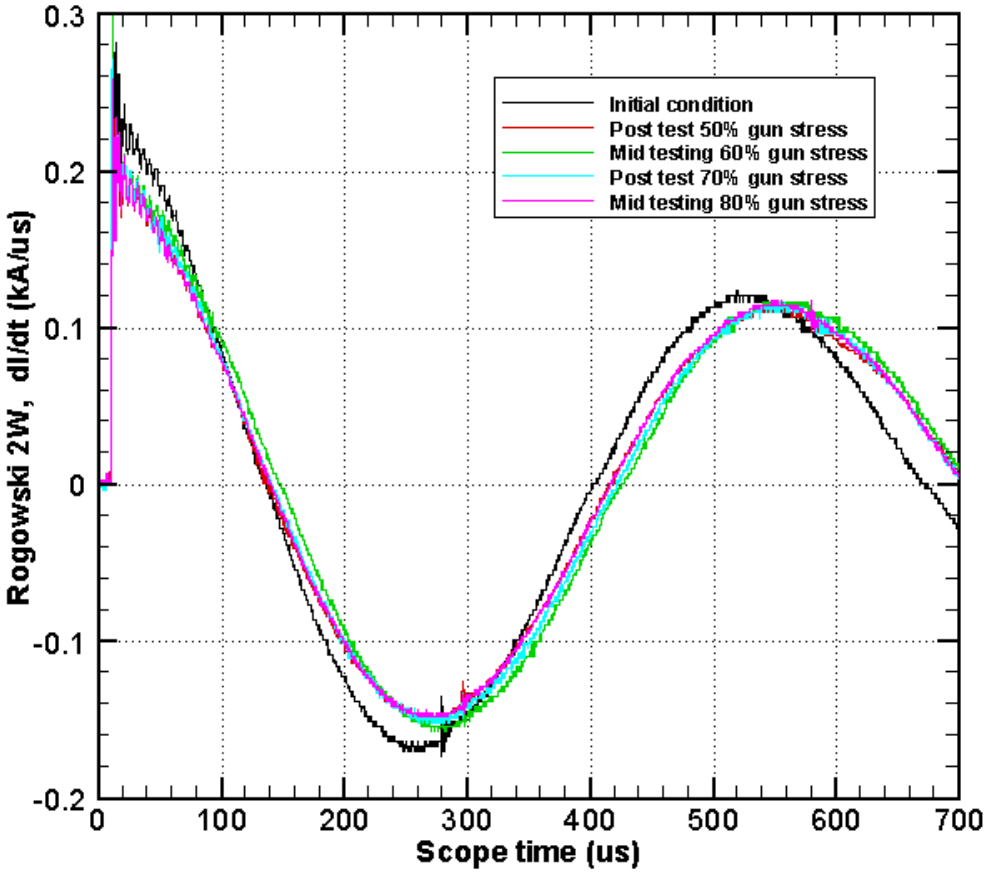

Figure 18. Waveforms of Rogowski probe 2W from ringing current tests of Coil 2 at 10% of gun stress level.

Examples of Rogowski probe data from a Coil 2 test at 80% gun stress level (50 kJ stored per bank) are shown in Figure 19. Both the probe data and the numerically integrated current are shown for each of the two feeds (East and West) delivering current to the coil.

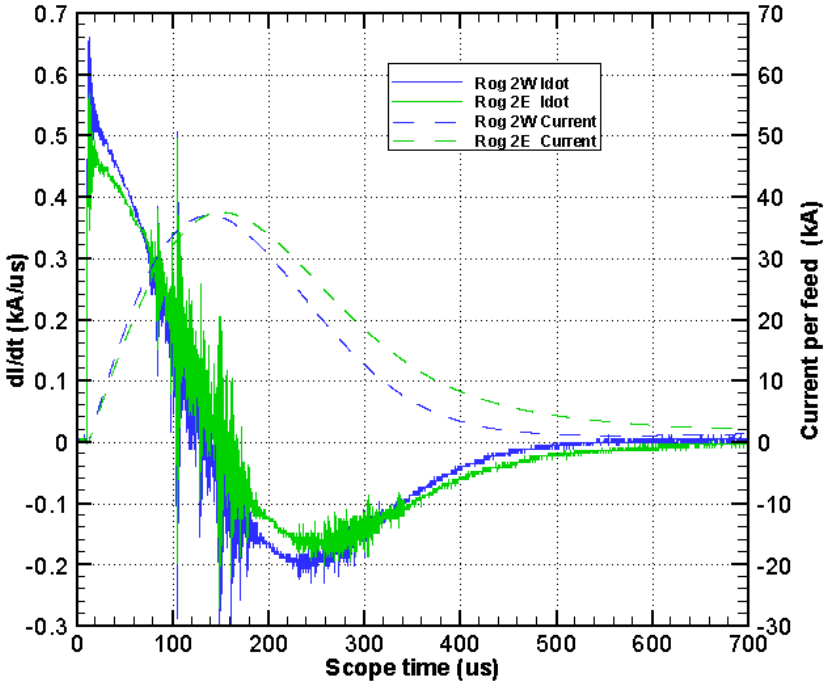

Figure 19. Rogowski probe data and numerically integrated current into each feed of Coil 2 tested at 80% of gun stress level.

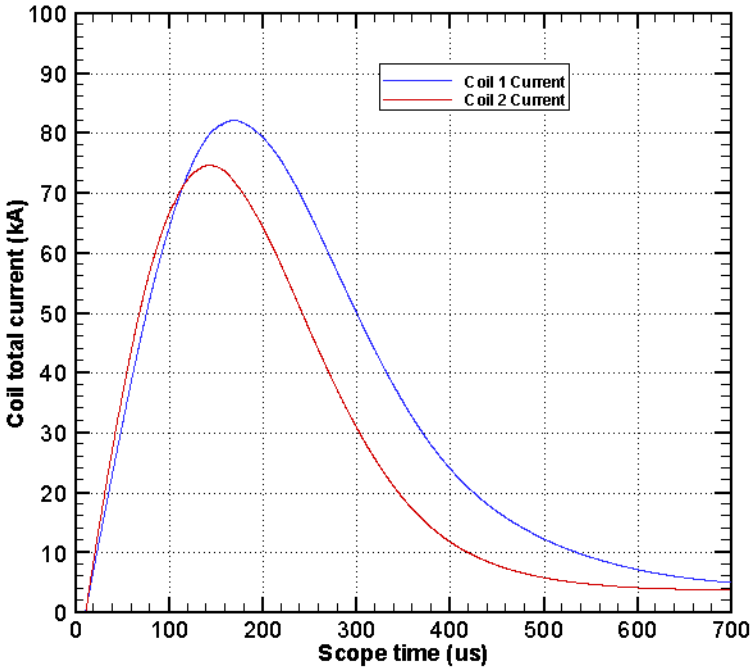

Figure 20. Current into each of the testbed coils for test at 80% gun stress level.

The total current waveforms in Figure 20 show the appropriate risetime, but the magnitude of the total current in Coil 2 is slightly lower than expected for 80% gun stress level. This is most likely due to limited signal resolution during the in-situ calibration of the probes prior to testing. Recalibration of the probes is planned. The magnitude of Coil 1 current is within 4% percent of the anticipated value. When comparing the total current data to the calculations in Figure 15, note that the data trace timebase is delayed 12 us.

Noise Pickup on Rogowski Probes

As indicated above, high frequency noise pickup on Rogowski probes has been previously used as an indicator of possible breakdowns in the wire insulation of litz cable coils. Typically the high frequency noise occurs near the time of peak current on the waveform, i.e., when the dI/dt signal crosses zero. However, this noise that modulates the fundamental current discharge from the bank can be due to any component in series with the coil. Such noise has been seen in the past due to electrical connections of feeds or cables that work loose during testing, although in this case, no loose connections were found.

The noise source in the testbed circuit is believed to be the main closing ignitron switch, SW1. The switches used in the banks have a previous shot history that is unknown going back to 1990-1993, although none are believed to be damaged. The noise level is also dependent upon the number of shots on that switch for a given day. In the first test of the morning, almost no noise is seen on Rogowski probes, but the noise level builds to that seen in Figure 19. A striking example of this is shown in Figure 21 where data from Shot 5, the last shot of the day at 80% gun stress level on 18sep03, is compared to the first test of the day on 19sep03 at the same energy level. If coil damage were the cause of this noise, there would be no recovery or healing overnight. The only other dynamic component in the circuit is the ignitron switch, and the quality of the mercury discharge in the switch appears to be shot dependent despite having forced-air cooling and operating in a low duty cycle. Such noise signatures were seen during operation of the 1993 coilgun and it was believed at that time that the coils of an earlier design might have been the cause. This data shows that may not have been the case.

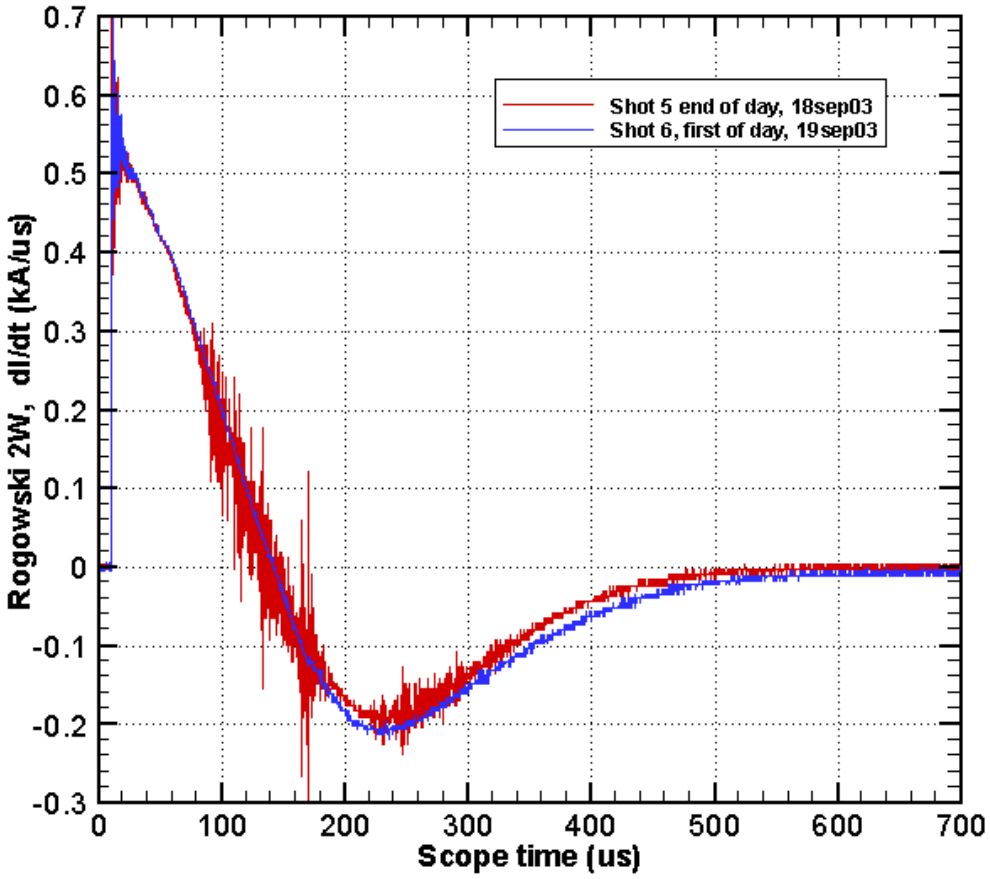

Figure 21. Comparison of Rogowski probe data from two sequential shots separated by an overnight period. If noise seen in Shot 5 were from the coil damage, the effect would be permanent.

Measurement of Projectile Thrust with Load Cell

To cross check the calculated thrust developed on the projectile, a load cell was placed in the structure of the testbed that locked the projectile in place. This cell was an ICP quartz force sensor, model 208CO5 from PCB Piezotronics connected to a PCB signal conditioner model 484B02 through about 16 m of 50 Ohm cable shielded with mu-metal conduit and copper braid. The thrust developed in the projectile was coupled to the load cell through a 4.4 cm diameter, 0.54 m long 7075-T6 aluminum rod held on axis in the barrel of the testbed. A static preload on the order of 0.5 to 1 kN kept the projectile in intimate contact with the load cell. This load cell has a frequency response of 36 kHz and a calibrated range for compressive loads up to 22.5 kN (5000 lbf).

Several problems arose with the data from the load cell measurements which are shown in Figure 22. The total current into Coil 2 is shown along with the force measurement on the same timebase. The lack of noise pickup on the base line of the load cell thrust measurement demonstrates that the shielding and careful configuration of cables to avoid ground loops was effective. The force signal is delayed about 135 us as expected for the transit time of the acoustic thrust signal traveling through the aluminum rod and spacers at 5 mm/us. The green curve is proportional to the square of the current waveform that has been timeshifted 145 us. This demonstrates the thrust force signature initially follows the expected temporal dependence. However, the magnitude of the thrust is approximately 60% of the anticipated value based on thrust calculated from Eq. 4 and measured inductance gradients. Additionally, the waveform does not then follow the expected form and "clips" at a level well below the limits of the cell, amplifier, or digitizers. Subsequent tests with the load cell demonstrated similar low output values with static loads. Therefore, additional testing with this diagnostic is planned in a calibrated test fixture before further thrust measurements are made and conclusions can be drawn from these data.

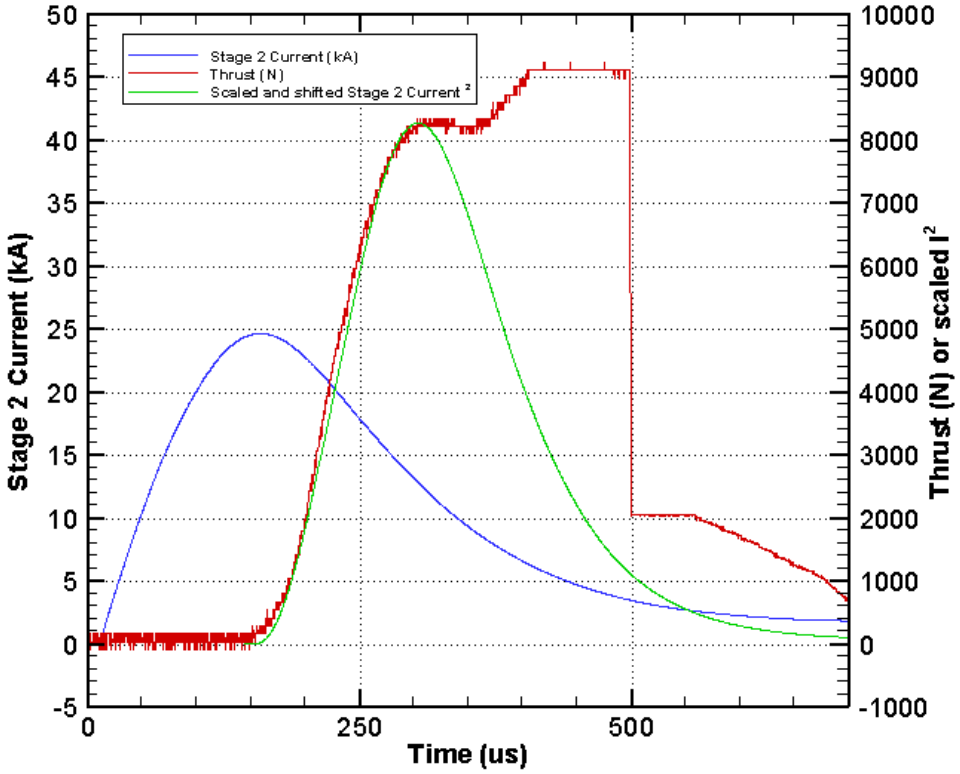

Figure 22. Coil 2 current and thrust force measured from load cell. While the thrust initially follows the time-shifted, current squared profile shown in green, the signal deteriorates and is not usable.

Conclusion

Coilguns have demonstrated their capability to launch projectiles to 1 km/s, and there is interest in their application for long-range precision strike weapons. These applications will require coil operation at the same 30 Tesla magnetic field strength as previously tested, but with bore diameters ranging from 100 to 300 mm, and mechanisms for heat rejection to accommodate firing rates of several shots per minute. The incorporation of a cooling system will impact the mechanical design and response of the future coils.

To assess the impact of such changes, an evaluation of the ruggedness and reliability of the existing 50 mm bore coil designed in 1993 was made by repeatedly testing at stress levels associated with operation in a coilgun. A two-coil testbed has been built with a static projectile where each coil is energized by its own capacitor bank. Simulation models of the applied forces generated in this testbed have been created with the SLINGSHOT circuit code to obtain loads equivalent to the worst-case anticipated in a 50 mm coilgun that could launch a 236 g projectile to 2 km/s.

Bench measurements of the seven remaining coils built in 1993 have been used to evaluate which coils were viable for testing, and only one was found defective. Measurements of the gradient of the effective coil inductance in the presence of the projectile were compared to values from SLINGSHOT, and the agreement is excellent. This indicates the prediction of thrust should likewise be very good. Load cell measurements of thrust were made, but problems with the diagnostic response preclude comparison to the calculations until a pulsed calibration of the cell can be conducted.

Repeated testing of the HFC5 coil built in 1993 has demonstrated no failures after 205 shots. These tests have been done in 50 shot groups from 50% to 90% of the stress levels anticipated in the 50 mm coilgun, stepping in 10% increments. This method was selected to obtain as many shots as possible on the coil while working below a known failure mechanism in the winding layer-to-layer transition at the 100% stress level. The number of shots achieved to date without a failure is an order of magnitude greater than any number achieved in previous testing in 1993. Although this testing has only been done on two coils, the results are encouraging as it demonstrates there are no fundamental weak links in the design that will cause a very early failure. The testing also demonstrates that the swaged litz cable-to-feed joint is quite robust even when slightly damaged in handling, and the joint design will be considered for future coils.

Several recommendations for future coil designs are suggested following the execution of this study.

1. A composite ring is recommended to reinforce the composite shells where the layer-to-layer transition essentially splits the shell in half at the ends of the winding. This ring should match the helical pitch of the winding to also provide axial support litz cable.

2. Feeds to the coils must be shortened to reduce the potential damage to the junction to the litz cable. Reducing the length proportionally reduces the moment that is applied to this critical connection.
3. Additional support is also needed at the litz cable-feed junction to prevent damage when the cables are attached and tightened. Ideally, this junction should be ruggedly molded into the body of the outer coil housing.
4. Future designs must consider embedded strain and temperature diagnostics to provide a state-of-health of the coil. This is difficult since the probes typically need to be fiber optic based for immunity to electromagnetic interference, and both the probe and its transmission line are fragile. Egress of the transmission line is problematic because of limitations to bend radius, but this may be accommodated by following the litz cable path. Regardless, any diagnostic that can provide information of impending coil failure has great value and should be pursued.
5. Additional static testing is needed up to the 100% gun stress level on the existing HFC5 model coils as funding and time permits to establish shot life and failure mechanisms other than the weak transition demonstrated in 1993.
6. Lifetime data for high field coils developed at the National High Magnetic Field Laboratory were not available in time for this study. That comparison should be made to provide a benchmark for lifetime characteristics and failure mechanisms in coils of similar construction and field strength.

References

1. S.Shope et al., “Long Range Naval Fire Support With a Coilgun,” Sandia National Laboratories Report, SAND2001-3832, February 2002.

2. R.J. Kaye et al., “Design and Evaluation of Coils for a 50 mm Diameter Induction Coilgun Launcher,” *IEEE Trans. Mag.*, vol. 31, no. 1, January 1995, pp. 478-483.

3. Kevlar is the trademark of the E.I. Du Pont de Nemours & Co., Inc., Wilmington, Delaware.

4. Nextel is the trademark of the 3M Corp., St. Paul, Minnesota

5. B.M. Marder, “SLINGSHOT – A Coilgun Design Code,” Sandia National Laboratories Report, SAND2001-1780, September, 2001.

Distribution

1	MS1165	William Guyton	15300
1	MS1153	Malcolm T. Buttram	15330
10	MS1182	Bobby N. Turman	15335
10	MS1182	Ronald J. Kaye	15335
10	MS1182	Gregory A. Mann	15335
1	MS9018	Central Technical File	8945-1
2	MS0899	Technical Library	9616